AIAA JOURNAL
Vol. 36, No. 5, May 1998

Technical Notes

TECHNICAL NOTES are short manuscripts describing new developments or important results of a preliminary nature. These Notes cannot exceed 6 manuscript pages and 3 figures; a page of text may be substituted for a figure and vice versa. After informal review by the editors, they may be published within a few months of the date of receipt. Style requirements are the same as for regular contributions (see inside back cover).

Comparison of Three Navier–Stokes Equation Solvers for Supersonic Open Cavity Simulations

Paul D. Orkwis*
University of Cincinnati, Cincinnati, Ohio 45221
Balu Sekar†
U.S. Air Force Research Laboratory, Wright–Patterson Air Force Base, Dayton, Ohio 45433
and
Sukumar Chakravarthy‡ and Oshin Peroomian§
Metacomp Technologies, Inc., Westlake Village, California 91361-2510

Introduction

TIME-accurate computations of open cavity flow physics and acoustic effects depend on a variety of factors including discretization technique, flux representation, flux limiters, turbulence model, grid resolution, boundary conditions, transient purge time, timestep, and code efficiency. The first author has produced a series of articles[1–4] that have explored the effect of boundary conditions, turbulence models, grid resolution, and transient purge times for a particular computational algorithm and timestep applied to compute a two-dimensional supersonic open cavity. However, many time-accurate unsteady codes are available for computing this class of flowfield, and the differences between the approaches are unclear. Temporal errors associated with solver discretization must be understood for a scheme to be used with confidence. In addition, it is unclear how one should choose the timestep given sufficient computational resources.

This Note compares the results obtained with an approximately factored lower–upper triangular solver, an explicit Runge–Kutta (RK) scheme, and a point implicit (PI) method for a variety of timesteps to assess solver error and timestep issues in computations of unsteady flows.

Numerical Methods

Two of the solvers used in the current work are contained in the CFD++ algorithm.[5,6] This code is a unified grid solver, i.e., in two dimensions one can use quadrilateral and/or triangular cells and in three dimensions hexahedral, triangular prisms and/or tetrahedral cells. However, in the current research it is applied only on structured grids for comparison purposes. The two solvers contained in the CFD++ algorithm are an explicit, temporally second-order RK approach and a temporally first-order PI method. The third solver is the Ruby code of Simpson and Whitfield[7] as modified by Tam et al.[2] It is characterized simply as a time-accurate, implicit finite volume technique, which utilizes Newton-like subiterations to achieve second-order temporal accuracy. All three solvers employ a Roe-type spatial flux difference splitting and continuous flux limiters. Several turbulence models are available in the codes. Unfortunately, there is no method that is common to both codes; therefore, the computations presented herein were obtained assuming a laminar flow.

The test case studied in the current work[8] was a simple two-dimensional turbulent cavity with a length-to-depth ratio of 2 and core flow conditions of $M_\infty = 2$ and $Re/m = 37.7 \times 10^6$. Grids, boundary conditions, and initial conditions followed those employed previously,[1–4] in which laminar solutions were also obtained.

Convergence to a cyclic state was assumed after a running average of data indicated the time-averaged sound pressure level $\overline{\mathrm{SPL}}$ and dominant frequency reached unchanging values. An oscillation cycle was defined from the pressure time history traces (Fig. 1) taken at the $x/L = \frac{2}{3}$ point on the cavity and was defined as the period between two pressure troughs (or peaks) occurring sometime after the transient purge period had passed. The pressure traces indicate clearly that significant transients occur up to approximately 20 characteristic times T_c and that a very regular oscillation cycle begins after approximately $40T_c$. The dominant frequency of oscillation was obtained directly from these data by taking the reciprocal of the time interval between the valleys (peaks). This produces a much smaller error than does running the signal through a fast Fourier transform, as only a relatively small amount of sampling data is available, compared with the experiments. Sound pressure levels were computed directly from the pressure data once the oscillation cycle was known.

Solver Error Study

The first goals of this work were to assess the differences in the flow physics obtained with the three schemes. The general results

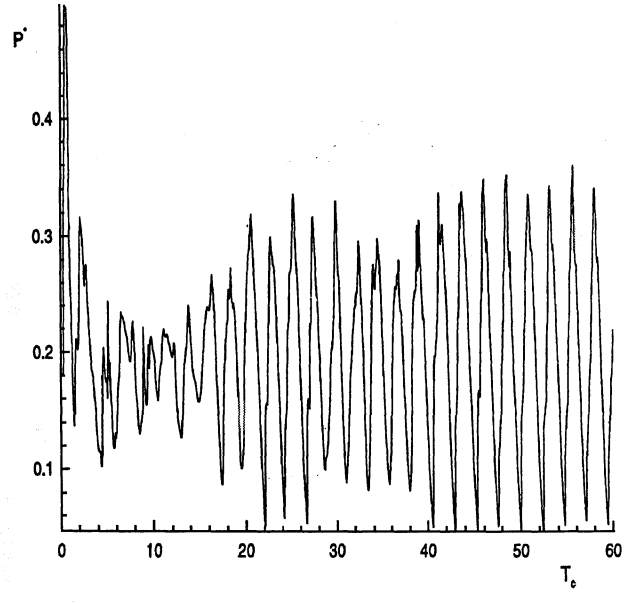

Fig. 1 Nondimensional pressure vs characteristic time at $x/L = \frac{2}{3}$ on the cavity floor: RK, CFL = 1.0.

Presented as Paper 97-3163 at the AIAA/ASME/SAE/ASEE 33rd Joint Propulsion Conference, Seattle, WA, July 6–9, 1997; received Aug. 13, 1997; revision received Jan. 30, 1998; accepted for publication Jan. 30, 1998.

*Associate Professor, Department of Aerospace Engineering and Engineering Mechanics. Senior Member AIAA.
†Aerospace Engineer, Propulsion Directorate, Turbine Engine Division, Components Branch. Associate Fellow AIAA.
‡Chief Scientist, 650 Hampshire Road, Suite 200. Senior Member AIAA.
§Scientist, 650 Hampshire Road, Suite 200. Senior Member AIAA.

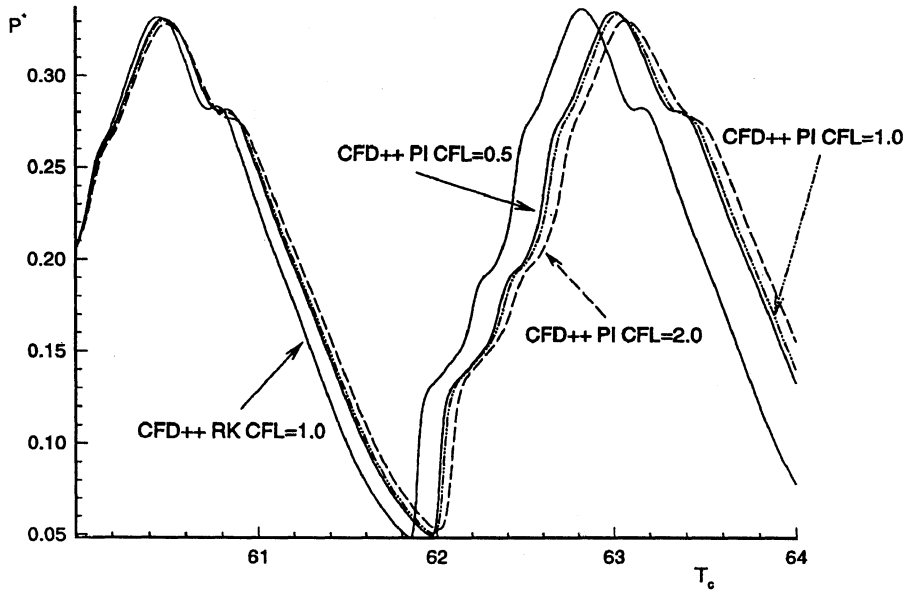

Fig. 2 Nondimensional pressure vs characteristic time at $x/L = \frac{2}{3}$ on the cavity floor: CFD++–RK, CFL = 1.0; and CFD++–PI, CFL = 0.5, 1.0, and 2.0; T_c = 60–64.

Table 1 Sound pressure level, dominant oscillation frequency results for Ruby, CFD++–RK, and CFD++–PI solvers and from experiment of Disimile and Orkwis[8]

Method	CFL	v_d, kHz	$\overline{\text{SPL}}$, dB
Ruby	0.1	26.6	174.5
CFD++–RK	0.1, 0.25, 0.5, 1.0	20.6	178.4
CFD++–PI	0.5	19.3	178.4
CFD++–PI	1.0	19.2	178.2
CFD++–PI	2.0	18.9	178.1
Experiment	Not applicable	23.0	164.5

showed that the physical mechanisms inherent in the flow were qualitatively the same for all three solvers and for all tested maximum Courant–Friedrichs–Lewy numbers ($\text{CFL}_{\max}$). Further details can be found in Ref. 9.

The quantitative results were somewhat different, as summarized in Table 1. Note that the three schemes straddle the dominant frequency v_d value found in the experiment but that all of the solvers predicted higher values of the $\overline{\text{SPL}}$. The v_d results from the CFD++ solvers were closer, by nearly 2 kHz, to the experiment than the Ruby results. As expected, the first-order PI scheme produced a lower v_d than either of the second-order schemes, an indication of greater temporal errors. Note that, when turbulence models were employed previously in the Ruby code,[4] the $\overline{\text{SPL}}$ decreased by as much as 20 dB and v_d increased by as much as 3 kHz from the laminar result. In those cases the general trend with increased turbulent dissipation was for the $\overline{\text{SPL}}$ to decrease and for v_d to increase. Hence, it is an indication of greater temporal accuracy as compared with the Ruby code that these laminar CFD++ results underpredicted v_d and overpredicted $\overline{\text{SPL}}$. Therefore, with the addition of a turbulence model, the CFD++ results should be markedly better than the corresponding turbulent Ruby code results. The current results show that solver differences have a significant effect on the $\overline{\text{SPL}}$ and v_d predictions even when similar spatial differencing, grids, and timesteps are employed.

Timestep Variation Studies

Timestep effects were tested in two ways in the current work. In the first approach, several schemes were tested from a time-zero initial condition. Results were obtained up to $60T_c$ for the RK scheme with $\text{CFL}_{\max}$ values of 0.5 and 1.0 and the PI scheme with $\text{CFL}_{\max} = 1$. The RK and PI solutions exhibited different transient purge behaviors (as evidenced by the pressure time histories), cyclically converged dominant frequencies, and sound pressure levels. However, the RK results were the same for both $\text{CFL}_{\max}$ values. That is, the RK cases both produced the same pressure time histories (to three-digit accuracy) from time zero to $60T_c$.

The second temporal test series was performed using the baseline $60T_c$ RK results as initial conditions for a series of RK and PI calculations. Figure 2 shows the pressure time histories from 60 to $64T_c$ for the RK scheme tested with $\text{CFL}_{\max}$ values of 0.1, 0.25, 0.5, and 1.0 and for the PI scheme with $\text{CFL}_{\max}$ values of 0.5, 1.0, and 2.0. (The RK method was unstable for $\text{CFL}_{\max} = 2.0$.) Of note in Fig. 2 is the conformity of the RK results, which again differed by only as much as three-digit accuracy throughout the oscillation cycle. Note that the $\overline{\text{SPL}}$ and v_d results for these cases match that obtained in runs started from time zero, which indicates that, if the method is temporally accurate, passing through the transient purge period in the most economical manner is advisable.

Figure 2 also shows differences between the PI and RK results, as well as the temporal convergence of the PI results with timestep reduction. It is clear that the PI scheme exhibits timestep convergence with continued timestep reduction but does not converge to the RK result. It is also apparent that the wave form amplitude is attenuated greatly with increased CFL for the PI scheme. These results illustrate the greater temporal error of the PI scheme compared with the RK scheme, indicating that the temporal solver can account for major differences in unsteady-flow statistics.

Conclusions

Solver differences were shown to be significant in the computation of complex unsteady flows. Whereas qualitative features were computed equally well with all schemes, definite quantitative differences in unsteady-flow statistics were found. In addition, timestep choice was shown to alter significantly the unsteady statistics for the point implicit scheme, although it had no effect on the explicit Runge–Kutta scheme. Timestep convergence was not exhibited by the point implicit scheme until the timestep fell below the maximum permitted by the Runge–Kutta solver, thereby negating the primary advantage of implicit solvers: significantly greater timesteps. The results have shown clearly that solver and timestep choice affect greatly the accuracy of unsteady-flow simulations and must be considered important, along with choice of grid, spatial discretization, and turbulence model.

Acknowledgments

The first author would like to thank the Aero Propulsion and Power Directorate, Advanced Propulsion Division/Propulsion Systems Branch (POPS) at the U.S. Air Force Research Laboratory for its financial support of this effort through the auspices of the 1996 Research and Development Laboratory/Air Force Office of Scientific Research Summer Faculty Research Program. Computational resources were supplied by the POPS, the Aeronautical Systems

Center and Army Research Laboratory, Department of Defense Major Shared Resource Centers, and the NASA National Aerodynamic Simulation program.

References

[1]Orkwis, P. D., Tam, C.-J., and Disimile, P. J., "Observations on Using Experimental Data as Boundary Conditions for Calculations," *AIAA Journal*, Vol. 33, No. 1, 1995, pp. 176–178.

[2]Tam, C.-J., Orkwis, P. D., and Disimile, P. J., "Comparison of Baldwin–Lomax Turbulence Models for Two-Dimensional Open Cavity Computations," *AIAA Journal*, Vol. 34, No. 3, 1996, pp. 629–631.

[3]Tam, C.-J., Orkwis, P. D., and Disimile, P. J., "Supersonic Open Cavity Flow Physics Ascertained from Algebraic Turbulence Model Simulation," *AIAA Journal*, Vol. 34, No. 11, 1996, pp. 2255–2260.

[4]Tam, C.-J., Orkwis, P. D., and Disimile, P. J., "Variations in Flow Field Physics Caused by Algebraic Turbulence Model Modifications for a Supersonic 2-D Open Cavity," AIAA Paper 97-0660, Jan. 1997.

[5]Chakravarthy, S., and Peroomian, O., *CFD++ User Manual, Version 96.07*, Metacomp Technologies, Westlake Village, CA, 1996.

[6]Chakravarthy, S., and Peroomian, O., *CFD++ Technical Reference*, Metacomp Technologies, Westlake Village, CA, 1996.

[7]Simpson, L. B., and Whitfield, D. L., "Flux Difference Split Algorithm for Unsteady Thin-Layer Navier–Stokes Solutions," *AIAA Journal*, Vol. 30, No. 4, 1992, pp. 914–922.

[8]Disimile, P. J., and Orkwis, P. D., "Effect of Yaw on Pressure Oscillation Frequency Within Rectangular Cavity at Mach 2," *AIAA Journal*, Vol. 35, No. 7, 1997, pp. 1233–1235.

[9]Orkwis, P. D., Sekar, B., Chakravarthy, S., and Peroomian, O., "Comparison of Three Navier–Stokes Equation Solvers for Supersonic Open Cavity Computations," AIAA Paper 97-3163, July 1997.

D. S. McRae
Associate Editor

Geometrical Effects on the Near-Field Flow Structure of Coaxial Jets

H. Rehab,* E. Villermaux,† and E. J. Hopfinger†
Centre National de la Recherche Scientifique, 38041 Grenoble Cedex, France

I. Introduction

COAXIAL jets have a wide range of applications and are used, for instance, in liquid propellant rocket engines, where a slow stream of liquid oxygen has to be mixed with a high-speed annular stream of gaseous hydrogen. When Reynolds numbers are high, the main parameter that governs the near-field development of the coaxial jets' flow is the ratio of the annular to the central jet momentum flux[1,2] $M = \rho_2 U_2^2/\rho_1 U_1^2$. This ratio reduces to the velocity ratio $r_u = U_2/U_1$ when the two streams are of equal densities. Depending on the value of r_u, the existence of two flow regimes has been demonstrated by Rehab et al.[1] The first one corresponds to the values of r_u in the range $1 < r_u < r_{uc}$ and is essentially characterized by the existence of a central potential core whose length is given by A/r_u, where A is a numerical constant. The other regime appears for $r_u > r_{uc}$, in which case the central potential core is chopped off and an unsteady recirculation bubble begins to form as shown in Ref. 2. It is to be expected that the numerical constant A and the threshold r_{uc} of the onset of the recirculating regime depend on initial conditions. These conditions are of two kinds: 1) the nozzle geometry, essentially characterized by the ratio of the outer to the inner nozzle diameters[3] $\beta = D_2/D_1$ and, possibly, the retraction of the inner nozzle with respect to the outer one, and 2) the exit conditions, i.e, the shape of the exit velocity profiles.[4] The Reynolds number, which fixes the mixing layer instability onset, acts only slightly on the inner core length provided it is large enough (10^4–10^5), which is generally the case in practice.[1] Dahm et al.[5] studied the case $r_u = 1$ in coaxial water jets with two different absolute values of the central and annular velocities. They showed the important effect of the wake behind the lip of the inner tube on the flow structure. In Ref. 1, it is shown that, when the velocity ratio is larger than unity, the inner mixing layer instability dominates the wake instability and the Reynolds number effect becomes very weak.

The present study focuses on the effects of the geometry of the coaxial injectors on the near-field flow structure. The dependence of the flow structure on the annular gap $e = (D_2 - D_1)/2$ is considered. The effect of the exit velocity profile is discussed. The consequences of a retraction of the inner tube on the coaxial jet flow dynamics is investigated too.

II. Experimental Setup and Methods

The experiments were conducted in a coaxial, axisymmetric water jet facility. The water is supplied by constant head tanks, and the jets issue into a large tank where water is at rest. Three coaxial nozzle configurations have been investigated. The long tube jet configuration is characterized by a fully turbulent pipe flow for the central jet and by a developed channel flow for the annular jet (at the nozzle exits). The diameter ratio is $\beta = 1.37$. The inner tube terminates, as is often the case in practical applications, with a divergence of a 6-deg angle and a lip thickness of 0.3 mm. The second configuration is similar to the first one but with the gap width increased; the diameter ratio is $\beta = 2.29$. In the third case, the jets emerge from convergent nozzles with contraction ratios of 2 and 4 for the central and the annular nozzles, respectively. The diameter ratio is $\beta = 1.35$.

The mean and fluctuation velocity measurements were made with constant-temperature, hot-film anemometers. The mean velocities at the nozzle exits are in the range $0 \le U_1 \le 1$ m/s and $0.3 \le U_2 \le 4$ m/s, giving Reynolds numbers on the order of 10^4–10^5. The measurement uncertainty for the velocity and the length scales [x_{p1} and $(x_{s2} - x_{s1})$] are 2.5 and 1%, respectively. For the critical velocity ratio, the uncertainty is approximately 5%.

III. Experimental Results

A. Effects of the Annular Gap Width

The mean axial velocity variations along the axis for different values of r_u have been measured, the outer velocity being fixed. The central jet potential core length x_{p1} is determined from the minimum in the mean velocity on the axis. In Fig. 1 the values of x_{p1} determined from the velocity minima are plotted as a function of r_u for the three geometries considered. It is observed that x_{p1} follows the relation $x_{p1}/D_1 = A/r_u$, with $-A$ a numerical constant equal to 6 for $\beta = 1.37$ and 7.5 for $\beta = 2.29$, so that for a given value of $r_u < r_{uc}$ the core length is longer when the gap is larger. Also, when the

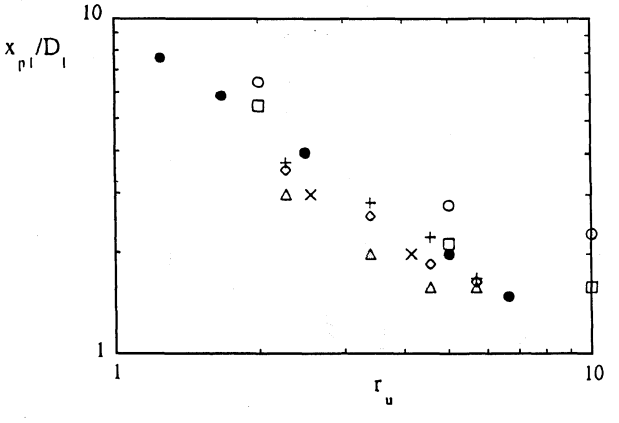

Fig. 1 Dependence of the central potential core on velocity ratio determined from the minima in axial velocity: Δ, $\beta = 1.37$; ◇, $\beta = 2.29$; and +, $\beta = 1.35$. Included for comparison: •, $\beta = 2$ (Au and Ko[6]); ×, $\beta = 1.4$ (Dahm et al.[5]); and □, $\beta = 1.51$ and 1.98 (Champagne and Wygnanski[3]).

Received Dec. 11, 1996; revision received Dec. 29, 1997; accepted for publication Jan. 29, 1998.

*Doctor, Laboratoire des Ecoulements Géophysiques et Industriels, Institut de Mécanique de Grenoble, B.P. 53X.

†Professor, Laboratoire des Ecoulements Géophysiques et Industriels, Institut de Mécanique de Grenoble, B.P. 53X.